PROBING THE ROLE OF DYNAMICAL FRICTION IN SHAPING THE BSS RADIAL DISTRIBUTION. I. SEMI-ANALYTICAL MODELS AND PRELIMINARY *N*-BODY SIMULATIONS

P. MIOCCHI[1], M. PASQUATO[2,3], B. LANZONI[1], F. R. FERRARO[1], E. DALESSANDRO[1],
E. VESPERINI[4], E. ALESSANDRINI[1], AND Y.-W. LEE[2]

[1] Dipartimento di Fisica e Astronomia, Università di Bologna, Viale Berti Pichat 6/2, I-40127 Bologna, Italy
[2] Department of Astronomy and Center for Galaxy Evolution Research, Yonsei University, Seoul 120-749, Korea
[3] Yonsei University Observatory, Seoul 120-749, Korea
[4] Department of Astronomy, Indiana University, Bloomington, IN 47405, USA
Received 2014 August 22; accepted 2014 November 5; published 2015 January 14

ABSTRACT

We present semi-analytical models and simplified *N*-body simulations with 10^4 particles aimed at probing the role of dynamical friction (DF) in determining the radial distribution of blue straggler stars (BSSs) in globular clusters. The semi-analytical models show that DF (which is the only evolutionary mechanism at work) is responsible for the formation of a bimodal distribution with a dip progressively moving toward the external regions of the cluster. However, these models fail to reproduce the formation of the long-lived central peak observed in all dynamically evolved clusters. The results of *N*-body simulations confirm the formation of a sharp central peak, which remains as a stable feature over time regardless of the initial concentration of the system. In spite of noisy behavior, a bimodal distribution forms in many cases, with the size of the dip increasing as a function of time. In the most advanced stages, the distribution becomes monotonic. These results are in agreement with the observations. Also, the shape of the peak and the location of the minimum (which, in most of cases, is within 10 core radii) turn out to be consistent with observational results. For a more detailed and close comparison with observations, including a proper calibration of the timescales of the dynamical processes driving the evolution of the BSS spatial distribution, more realistic simulations will be necessary.

Key words: blue stragglers – globular clusters: general – methods: analytical – methods: numerical – stars: kinematics and dynamics

1. INTRODUCTION

Globular clusters (GCs) are dynamically active systems that, within the timescale of the age of the universe, undergo nearly all of the physical processes known in stellar dynamics (Meylan & Heggie 1997). Gravitational interactions and collisions among single stars and/or binaries are quite frequent, especially in the highest density environments (e.g., Hut et al. 1992). They can also generate populations of exotic objects, like X-ray binaries, millisecond pulsars, and blue straggler stars (BSSs; see, e.g., Paresce et al. 1992; Bailyn 1995; Bellazzini et al. 1995; Ferraro et al. 2001, 2009; Ransom et al. 2005; Pooley & Hut 2006).

GCs are also old systems where all stars more massive than $\sim 0.8\,M_\odot$, the typical main sequence turn-off (MS-TO) mass, should have already exhausted their core hydrogen reservoirs and evolved toward the sub-giant branch or later phases. Nevertheless, in all well-studied GCs (e.g., Sandage 1953; Ferraro et al. 1992, 1999) BSSs are observed as a population of core hydrogen-burning stars along an extrapolation of the MS, in a region of the color–magnitude diagram (CMD), which is bluer and brighter than the MS-TO. Their position in the CMD and direct measurements suggest that these objects are more massive than the MS-TO stars, with typical masses of $\sim 1.2\,M_\odot$ (Shara 1997; Gilliland et al. 1998; De Marco et al. 2005; Ferraro et al. 2006a; Lanzoni et al. 2007b; Fiorentino et al. 2014). To solve this apparent paradox, two main mechanisms for the formation of BSSs have been proposed, both involving close physical interactions among stars: mass transfer in primordial binary systems (McCrea 1964; Zinn & Searle 1976) and direct collisions between unbound stars (Hills & Day 1976). The two formation channels could be at work simultaneously within the same cluster, probably depending on the local density (e.g.,

Fusi Pecci et al. 1992; Bailyn 1992; Ferraro et al. 1995, 2009). However, their relative efficiency is still a matter of debate (e.g., Sollima et al. 2008; Knigge et al. 2009; Chatterjee et al. 2013; Sills et al. 2013, see also Hypki & Giersz 2013) and distinguishing BSSs formed by either of the two mechanisms is a very hard task. The only notable exceptions are the detection of spectroscopic signatures of the mass transfer process in 47 Tucanae and M30 (Ferraro et al. 2006a; Lovisi et al. 2013, respectively) and the discovery of two distinct BSS sequences, likely connected to the two formation processes, in M30 and NGC 362 (Ferraro et al. 2009; Dalessandro et al. 2013b, respectively).

BSSs are also considered to be powerful probes of GC internal dynamics (e.g., Bailyn 1992; Ferraro et al. 1995, 1999, 2003, 2006b; Davies et al. 2004; Mapelli et al. 2004, 2006). In particular, Mapelli et al. (2006) first noted that, in some GCs, the position of the minimum of the BSS radial distribution nicely corresponds to the radius where the dynamical friction (hereafter DF) time equals the cluster age. Ferraro et al. (2012) put this observable in an evolutionary context, connecting the shape of the observed BSS radial distribution with the cluster dynamical age, thus defining the so-called dynamical clock, a fully empirical tool that is able to measure the stage of dynamical evolution reached by these stellar systems. In most of the surveyed GCs, the number of BSSs, normalized to the number of stars in a reference population (like sub-giants, red giants, or horizontal branch stars), shows a bimodal behavior as a function of radius: it is peaked in the center, has a dip at intermediate radii, and rises again in the cluster outskirts (e.g., Ferraro et al. 1993; Lanzoni et al. 2007a; Beccari et al. 2013, and references therein). A similar behavior has also recently been found in the extra-Galactic GC Hodge 11 in the Large

Magellanic Cloud (Li et al. 2013). In a few other cases, the BSS radial distribution shows only a central peak (Ferraro et al. 1999; Lanzoni et al. 2007b; Ferraro et al. 2009; Contreras Ramos et al. 2012), while in ω Centauri, NGC 2419 and Palomar 14 (Ferraro et al. 2006b; Dalessandro et al. 2008; Beccari et al. 2011, respectively) it is equal to the radial distribution of the normal cluster stars. Such a flat BSS radial distribution has also been found in dwarf galaxies (Mapelli et al. 2009; Monelli et al. 2012). Indeed, the comparative analysis performed by Ferraro et al. (2012) in a sample of 21 Galactic GCs demonstrates that these stellar systems can be grouped on the basis of the shape of their BSS radial distribution, each group corresponding to families of different dynamical age. The interpretative scenario is the following.

Being significantly more massive than normal cluster stars, BSSs are expected to experience a relatively fast segregation process, mainly as a "natural" consequence of the action of DF, that makes them progressively sink toward the cluster center. In general, a "test" star of mass m_t, orbiting at an average radius r in a field of lighter stars with average mass $\langle m \rangle$ decays toward the cluster center over a time

$$t_{df}(r) \simeq \frac{\langle m \rangle}{m_t} t_r(r), \tag{1}$$

where $t_r(r)$ is the relaxation time at the mean orbital radius r. Clearly, once the other parameters are fixed, the larger the value of m_t, the faster the object sinks to the center. Moreover, t_r is expected to increase with radius, because of its dependence on local density and velocity dispersion (see, e.g., Binney & Tremaine 1987). Therefore, heavy stars (as BSSs) orbiting at large $\langle r \rangle$ will decay extremely slowly, virtually unaffected by DF (unless they are on very eccentric orbits). Instead, BSSs that are closer to the center will decay quickly. On the other hand, because of their smaller masses, the reference population stars will be less affected by DF, compared to BSSs. It is thus reasonable to expect that, over time, the region in which the normalized BSS fraction (n_{BSS}/n_{ref}) is depleted by DF extends increasingly outward. In that region, the behavior of the local BSS fraction exhibits an absolute minimum (at r_{min}) between a central peak (made up of BSSs already decayed, plus collisional BSSs formed there) and an external rising branch (due to BSSs that have not had enough time to appreciably decay to the center).

Thus, it is reasonable to expect that in dynamically young clusters the minimum of the BSS radial distribution should be close to the center, while for increasing dynamical age, it should be observed at larger and larger distances. Therefore, r_{min} can be used as the hand of a "clock," able to measure the stage of the dynamical evolution reached by stellar clusters, with DF being the internal engine of this clock (of course, for a meaningful comparison among different clusters, r_{min} has to be normalized to a characteristic scale length, as the core radius r_c). Such a tool would also allow us to recognize cases where the relaxation process has not started yet,[5] from those where it is more advanced, possibly even close to the core-collapse (CC) phase. It may even help to distinguish between systems with a central density cusp due to CC, from those with a cusp due to an intermediate-mass black hole. The empirical indication of the validity of this simplified, DF-based, picture is provided by the

tight correlation found between the position of the minimum in the observed BSS radial distribution and the relaxation time computed at the core or at the half-mass radius (see Figure 4 in Ferraro et al. 2012). The trend has been also confirmed by additional observational studies (see Dalessandro et al. 2013a, 2013b; Beccari et al. 2013; Sanna et al. 2014).

From the theoretical side, Monte-Carlo and N-body simulations have been used to study the radial distribution of BSSs in GCs (Mapelli et al. 2004, 2006; Hypki & Giersz 2013; Chatterjee et al. 2013) and binary systems in open clusters (Geller et al. 2013). Indeed, these are the main routes to evaluate the role of DF in shaping the BSS distribution, since they offer deep insights on the influence of other important collisional phenomena, like those associated with close encounters and "binary burning" (mainly taking place close to, or immediately after, the cluster CC). Therefore, our group is adopting numerical approaches with gradually increasing levels of realism, in order to precisely evaluate and disentangle the role of the various dynamical mechanisms involved. In Alessandrini et al. (2014), we used a coupled analytical/N-body approach in the specific case of BSSs in a GC (i.e., test particles only slightly more massive than the average, orbiting a background field with a mass spectrum), to ascertain that the observed bimodalities cannot be due to a non-monotonic radial behavior of the DF timescale.

Here we first discuss a semi-analytical approach to the problem, assuming that DF is the only process driving the BSS secular evolution (Section 2). Then, we present collisional N-body simulations to take into account further dynamical mechanisms playing a role in determining this evolution (Section 3). Discussion and conclusions are presented in Section 4.

2. SEMI-ANALYTICAL MODELS

2.1. Basic Assumptions

We neglect BSSs formed through stellar collisions and only deal with the population generated by mass transfer activity in binary systems. We further assume that BSS progenitors are dynamically inert hard binaries, meaning that they suffer only from the effect of DF, and, moreover, their probability to actually become BSSs is independent of the cluster environment. Under these assumptions, we can model the BSS progenitors as point particles with masses equal to the sum of the binary components. Moreover, we assume that the progenitors that eventually give rise to BSSs are, at any time, just a random subsample of the overall progenitor population: hence, at any time, the radial distribution of these binaries well represents that of actual BSSs. In other words, it is assumed that BSSs and their binary progenitors (that we assume to be point particles) are indistinguishable.

Moreover, we consider the cluster to be an isolated system, with a discrete mass spectrum consisting of only three species, which are meant to represent MS stars below the TO (the lightest component, which primarily contributes to both the overall gravitational potential and DF), BSSs (the most massive component), and the reference population (the component with intermediate-mass stars and to which BSS star counts are normalized, corresponding to red-giants or horizontal branch stars in observational studies).

2.2. The Models

As a first step in understanding the specific role of DF in shaping the observed BSS radial distributions, we followed

---

[5] Note that this method, involving relatively bright stars, is much more effective than any other approach proposed thus far to measure the level of mass segregation (or the lack thereof).

a semi-analytical approach in which other simplifying assumptions are adopted in addition to those discussed above.

We considered here the cluster dynamics governed by a static "mean" gravitational field (Ψ), due to MS stars ("field" stars) only. We then assumed that Ψ remains fixed in time and is generated by a constant, spherically symmetric and isotropic distribution of field stars, each of which is assumed to have a mass m. Their phase-space distribution $f(r, v)$ is defined such that $f(r, v)\mathbf{dr dv}$ is the number of these stars in the phase-space volume element $\mathbf{dr dv}$ (with $r = |\mathbf{r}|$ and $v = |\mathbf{v}|$).

Within this field, we considered the evolution of the stars in the two heavier components (that we call "test" stars) under the effects of the DF against field stars. We neglected the self-gravity acting on all of these components, as well as any interaction between test stars. Hence, the stellar motion of any test star, with mass m_t, position $\mathbf{r}$, and velocity $\mathbf{v}$, is determined solely by the underlying gravitational field Ψ and by the DF deceleration that we describe following the Chandrasekhar (1943) formula (see, e.g., Binney & Tremaine 1987)

$$\mathbf{a}_{df} = -4\pi \ln \Lambda G^2 m(m + m_t)g(r, v)v^{-3}\mathbf{v}, \qquad (2)$$

where

$$g(r, v) \equiv 4\pi \int_0^v f(r, w)w^2 \mathrm{d}w \qquad (3)$$

is the number density at radius r of field stars moving more slowly than the considered test star. Assuming that field stars are distributed according to the Plummer (1911) distribution function with a fixed scale length r_0, an analytical expression (see Equation (A5) in the Appendix) can be derived for $g(r, v)$, while the gravitational field is given by

$$\Psi(\mathbf{r}) = -\frac{GM}{\left(r^2 + r_0^2\right)^{3/2}}\mathbf{r}, \qquad (4)$$

with M being the total mass in the field star component. Thus, once numerical values for m, m_t, M, and r_0 are chosen, the DF deceleration acting on BSSs and the reference stars is completely determined. In particular, we assigned to BSSs a mass of $3m$ and to the reference population stars a mass of $2m$. In physical units, this choice can be thought to correspond to $m = 0.4\,M_\odot$ for the mean stellar mass below the MS-TO, $0.8\,M_\odot$ for stars in the reference population and $1.2\,M_\odot$ for BSSs, all being appropriate values for the case of Galactic GCs.

As initial conditions for the time evolution of the two evolving components, we generated a set of $N_{\mathrm{BSS}} = 300$ and a set of $N_{\mathrm{ref}} = 1200$ positions and velocities for their representative particles, following the same Plummer distribution function used for the field stars. Of course, in real clusters, the relative abundance of BSSs with respect to the reference population is much lower than it is assumed here. However, such a large number of BSSs is adopted to limit the Poisson noise. To this end, we also generated 20 sets of initial conditions by changing only the random seed, and we then merged the snapshots of the resulting simulations after reporting the center of mass of each snapshot onto the origin of the coordinates. In addition, for each particle in each snapshot, we merged the three projections (along each coordinate axis), thus obtaining (from a statistical point of view) three times more stars. In this simplified approach, such an overabundant BSS population has no consequences on the system evolution, while it gives some spurious effects in the N-body simulations, which we will discuss later in Section 3.1. The assumption of the same initial distribution function for both
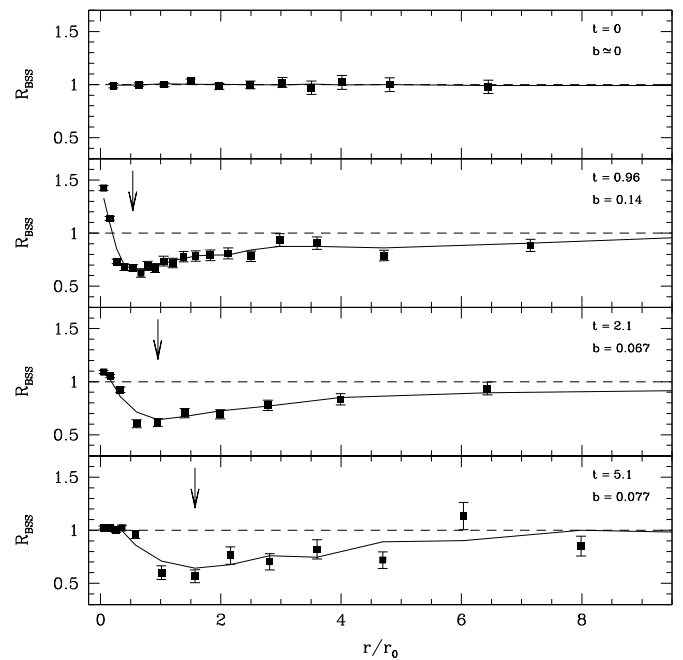
Figure 1. Double-normalized ratio (R_{BSS}) between the projected number of BSSs and that of reference stars, in various radial bins around the cluster center and at different evolutionary times (see labels), that were found from the semi-analytical simulations. Time is expressed in units of the half-mass relaxation time t_{rh}. The solid curve is the running average of the R_{BSS} radial behavior. Also labeled is the slope (b) of the rising branch beyond the dip (see the text). The number of radial bins is variable due to the employed adaptive binning method.

kinds of particles and the field component is empirically justified by observations: in fact, BSSs are found to share the same radial distribution as normal cluster stars in dynamically young GCs, where DF has not been effective yet in segregating massive stars toward the cluster center (see the cases of ω Centauri, NGC 2419, and Palomar 14 in Ferraro et al. 2012, and references therein).

Starting from these initial conditions, the orbit of each test star, evolving under the total acceleration $\mathbf{a} = \Psi + \mathbf{a}_{df}$, was time-integrated by means of a second order leapfrog algorithm (e.g., Hockney & Eastwood 1988) with a constant time step. At given times, a snapshot of the system was extracted and the projected number distribution of the two heavier stellar species was derived in a series of concentric annuli around the cluster center. To further improve the statistics, we superimposed the positions of the test particles in all 20 realizations, as well as their projections on the three coordinate planes (similarly to what was done in the N-body model, see Section 3).

2.3. Results

Consistently with the observational quantities defined in Ferraro et al. (1993), in Figure 1, we plot the "double-normalized" BSS radial distribution $R_{\mathrm{BSS}}(r) \equiv (n_{\mathrm{BSS}}(r)/N_{\mathrm{BSS}})/(n_{\mathrm{ref}}(r)/N_{\mathrm{ref}})$, i.e., the ratio between the relative fraction of BSSs and that of reference stars in each radial bin, at various evolutionary times. The radial distance is expressed in units of r_0, while times are in units of t_{rh}, namely the relaxation time computed at the half-mass radius (Binney & Tremaine 1987, Equation (8.72)) of the field star system: $r_h = r_0(2^{2/3} - 1)^{-1/2} \simeq 1.3r_0$ for the Plummer distribution.

To guarantee both a good radial sampling and a large enough number statistic, we set a minimum threshold (n) to the number of BSSs and a minimum threshold (Δr) to the width of each
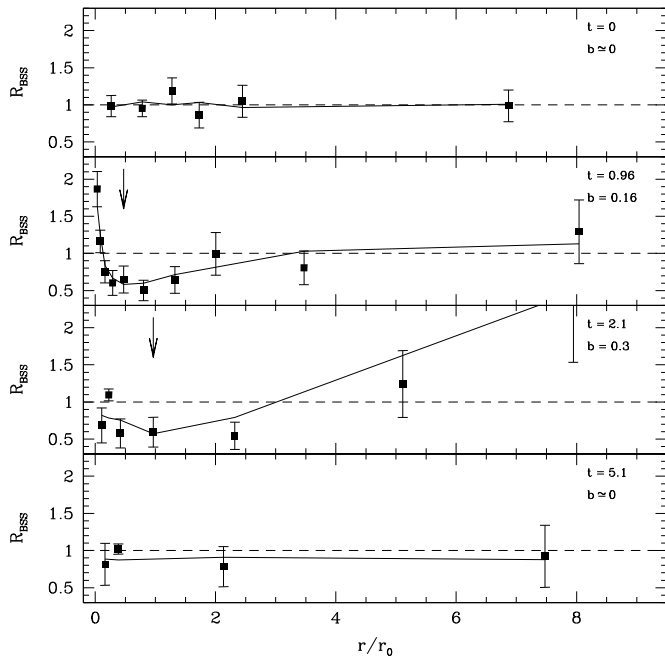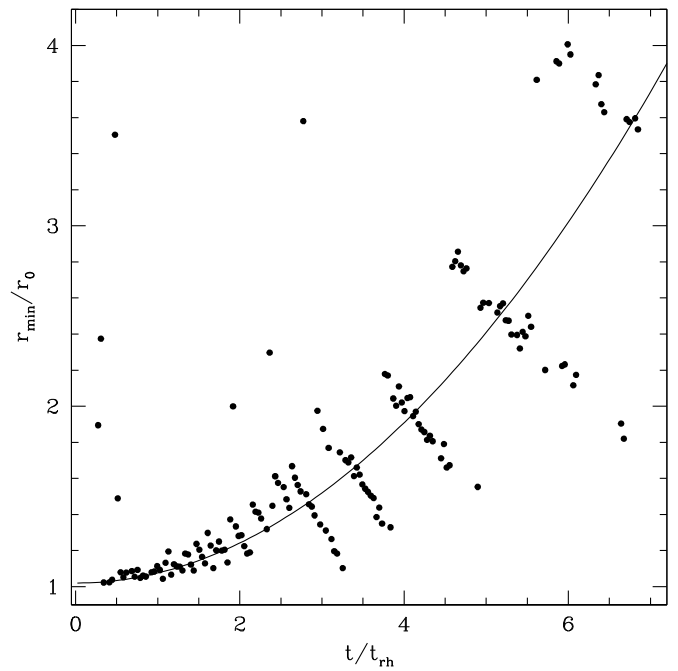
Figure 2. Same as in Figure 1, but considering the snapshots of only one simulation and with no merging of coordinate planes.

Figure 3. Time evolution of the position of the absolute minimum, $r_{\min}$ (dots), normalized to the Plummer characteristic scale radius, for all the snapshots in which $R_{\rm BSS}(r)$ has an appreciable bimodality ($b \gtrsim 0.01$; see the text). The solid line is a fitting $\sim t^2$ law.

radial bin. Then, the actual width of each bin was automatically determined as the minimum value larger than Δr such that $n_{\rm BSS} \geqslant n$ in that bin. In Figure 1, we chose $n = 300$ and $\Delta r = 0.1r_0$ for all times, except at late stages ($t = 5.1$), where $n = 100$ was used in order to get enough resolution also in the outer regions where the number of BSSs is quite small, and for $t = 0$ where $\Delta r = 0.4r_0$. Uncertainties on the number ratios were estimated from the law of propagation of errors, assuming a Poissonian statistic for $n_{\rm BSS}$ and $n_{\rm ref}$.

For illustrative purposes, Figure 2 shows the $R_{\rm BSS}(r)$ profiles obtained by considering only one simulation in one projection direction. For obvious reasons, in doing this plot we had to reduce the BSS number bin threshold, n, by a factor of $\simeq 10$ and Δr by a factor of a few times. Unsurprisingly, with respect to Figure 1, a strong increase of the Poisson noise can be seen, especially in the outer regions where the number of particles is the lowest. This example illustrates the importance of reducing counting noises, which was done when applying the averaging procedure described above.

In order to properly characterize the shape of the $R_{\rm BSS}$ distribution and the location of its minimum ($r_{\min}$) in each snapshot, we first computed the running average[6] $\langle R_{\rm BSS}(r)\rangle$, with the aim of reducing fluctuations due to poor statistics. Then, $r_{\min}$ was defined as the distance from the cluster center of the absolute minimum of this average. While a flat behavior is set by construction at the initial time, a bimodality rapidly develops (see Figure 1). Moreover, the minimum of the normalized BSS radial distribution progressively drifts outward at increasing evolutionary times (note that r_0 is constant by construction in these Plummer models), until an almost flat behavior is established at late stages ($t \gtrsim 10t_{\rm rh}$). These results qualitatively confirm what was suggested by the intuitive picture discussed above, namely that DF by itself can give rise to a bimodal BSS distribution. On the other hand, we note that although a central peak begins to develop from the very beginning, it is

then rapidly leveled-off, at odds with what is observed in real clusters. This is because, in this simplified model, the frictional decay of both kinds of test stars continue indefinitely with an unaltered efficiency, thus causing the great majority of these stars to eventually decay to the innermost radial bins where, as a consequence, the peak in $n_{\rm BSS}/n_{\rm ref}$ is dumped to nearly its initial value (i.e., $R_{\rm BSS} = 1$). Indeed, the innermost five bins ($r/r_0 < 1$) in the bottom panel of Figure 1 contains $\sim 95\%$ of the total test stars.

To quantify the level of bimodality of the distribution, we defined the parameter b as the slope of the line that best-fits $\langle R_{\rm BSS}(r)\rangle$ in the region of the rising branch (specifically for $r_{\min} \leqslant r \leqslant r_{\min} + 4\Delta r$). A visual inspection of the snapshots indicates that the dip in $R_{\rm BSS}(r)$ can be well appreciated when $b \gtrsim 0.01$.[7]

The time behavior of $r_{\min}$, as measured in all distributions having $b \geqslant 0.01$, is plotted in Figure 3. From the inspection of this figure, we can state that (despite the large fluctuations): (1) the $R_{\rm BSS}$ radial behavior shows a significant level of bimodality most of the time for $0.5 \lesssim t/t_{\rm rh} \lesssim 7$; (2) there is a clear tendency of $r_{\min}$ to drift outward. The gaps among groups of $r_{\min}$ values shown in this figure (e.g., between $t/t_{\rm rh} \simeq 4.2$ and $\simeq 5.5$), as well as the linear anti-correlation within these groups, are an effect of the adaptive binning procedure.

3. N-BODY SIMULATIONS

To get deeper insights into the role played by DF and, possibly, other collisional effects on the observed shape of the BSS normalized radial distribution, we followed a more realistic approach, making use of self-consistent, collisional

---

6 It is a simple and central moving average with a window width of three bins.

7 We note, however, that an automatic parameterization of the bimodality is not an easy task since the shape of the region where the minimum of the distribution is located significantly changes with time. In particular, at late stages of the cluster evolution, this region broadens and the b parameter tends to become less sensible and easily loses the bimodal behavior.

N-body simulations. The same basic assumptions outlined in Section 2.1 have been adopted.[8] Nevertheless, here we have an accurate and self-consistent dynamical treatment of the various fully interacting stellar components, naturally including DF and close encounters, which are responsible for various dynamical phenomena (e.g., Meylan & Heggie 1997; Heggie & Hut 2003).

The simulations were performed using the direct N-body code NBODY6 (Aarseth 2003) with its Graphic Processing Unit extension enabled. We adopted the "Hénon units" (also known as N-body units) discussed in Heggie & Mathieu (1986), where $G = M = -4E = 1$, with G being the gravitational constant, M the total GC mass, and E the total GC energy (the sum of potential and kinetic energy, negative for a bound system). In these units, the half-mass relaxation time is (Giersz & Heggie 1994):

$$t_{\rm rh} = \frac{0.138 N r_h^{3/2}}{\ln(0.11N)}, \tag{5}$$

where N is the total number of particles (stars). While $t_{\rm rh}$ varies during the evolution because of the changes in both r_h and N (a star is removed from the system when its total energy is positive and it is outside $10 r_h$; see Aarseth 2003, Section 9.6), in the following, the time will be measured in units of $t_{\rm rh}$ as evaluated from the initial conditions (at $t = 0$). Note, finally, that, due to the freedom of scaling the simulation from Hénon to physical units, only the mass- and number-ratios of the species are relevant to the dynamics of the system, given the total number of stars.

3.1. Setting up the Simulations

We fixed the total number of stars to $N = 10^4$. Moreover, the same initial conditions were adopted for the three mass components: at $t = 0$, they all follow a King (1966) model with the same central dimensionless potential W_0 and King radius. Such as in the semi-analytical models, this corresponds to assuming no initial mass segregation and an observationally justified flat radial distribution for the ratio between the number of BSSs and that of reference stars initially. To check for possible dependences of the results on the initial cluster concentration, we ran three sets of simulations for three different values of W_0, namely $W_0 = 4, 6, 8$ (corresponding to King concentration parameters $c \sim 0.84, 1.2, 1.8$, respectively).

As in the semi-analytical model, we assumed the reference population stars to have a mass of $m_{\rm ref} = 2m$, and BSSs to have masses of $m_{\rm BSS} = 3m$. The relative number of the three species is more tricky, since real clusters' BSSs are numerically negligible with respect to the other two populations, but here a high-enough statistic is needed to obtain meaningful results. We therefore assumed $N_{\rm MS} = 8500$ and, as in Section 2, $N_{\rm ref} = 1200$ and $N_{\rm BSS} = 300$, in order to get a reasonable compromise between realistic values and a good statistical sampling. As was done in the model of Section 2, in this case, we also generated 20 sets of initial conditions and merged the snapshots of the resulting simulations, as well as the projections on the coordinate planes, in order to obtain, at any sampled time, a "super-snapshot" made up of $20 \times 3 \times 10^4 = 6 \times 10^5$ particles.[9] The unrealistically high fraction of BSSs increases
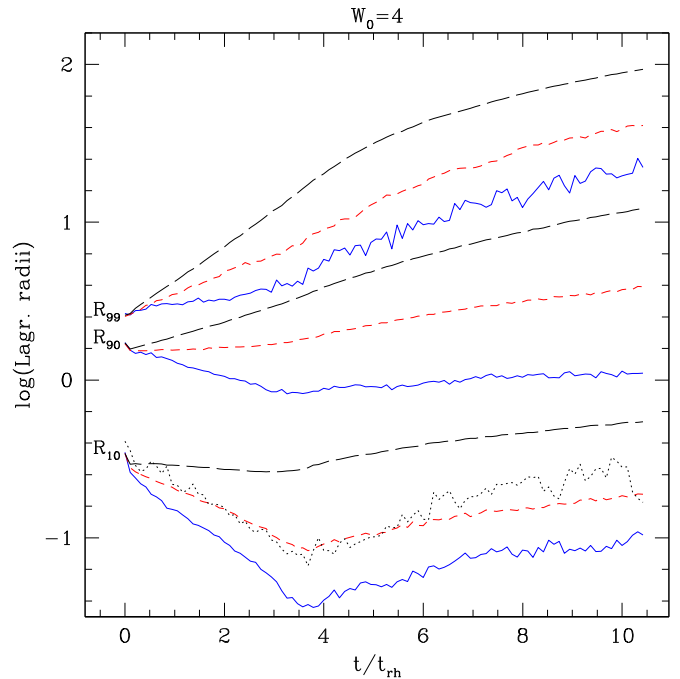
Figure 4. Evolution of three Lagrangian radii, R_p (expressed in Hénon units), enclosing the indicated percentage, p, of the total mass, for the three stellar components in the simulations started with $W_0 = 4$: BSSs (solid blue line); reference component (short-dashed red line); MS stars (long-dashed line). The dotted line represents the behavior of the core radius of the reference component, $r_c(t)$. For the sake of clarity, one in every 20 snapshots ($\sim t_{\rm rh}/10$) are considered in this plot.

the collisionality of the system in the central region, with the effect of making the evolution toward the CC faster. Nonetheless, in this preliminary study, we preferred to keep the statistical fluctuations low, even at the price of assuming a less realistic fraction of BSSs. However, in order to determine the importance of the enhanced collisional effect that this choice implies, an additional, more realistic, cluster model with $N = 10^5$ (and $N_{\rm ref} = 3000$, $N_{\rm BSS} = 300$) was also considered but, due to the huge computational costs, no statistical sampling was possible for the initial conditions and only one simulation (with $W_0 = 8$) was performed in this case.
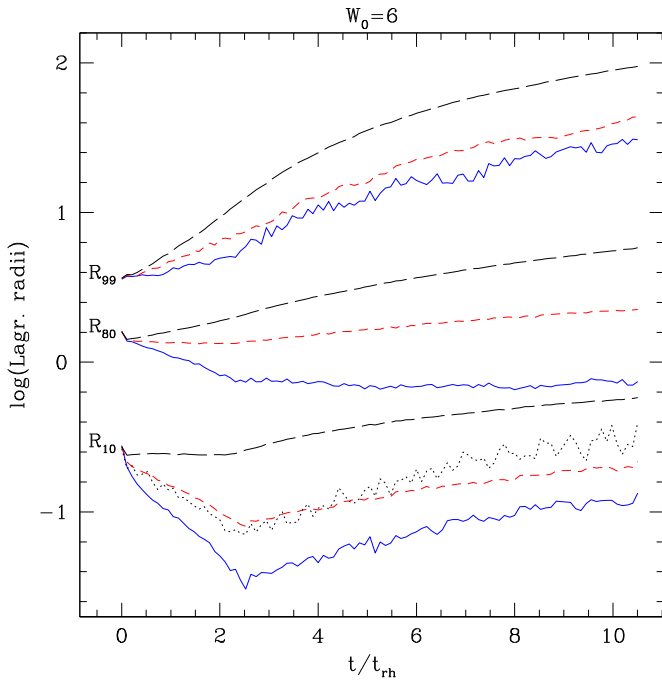
All simulations were run for several initial half-mass relaxation times or until NBODY6 failed to meet the desired minimal energy conservation accuracy (we set the $Q_{\rm E}$ parameter in NBODY6 input file to 10^{-4}; see Aarseth 2003). We then extracted a snapshot per Hénon unit of time. Since the typical crossing time of our models is of the order of several Hénon time units, this ensures that the evolution of individual star orbits is tracked in a relatively fine-grained way.
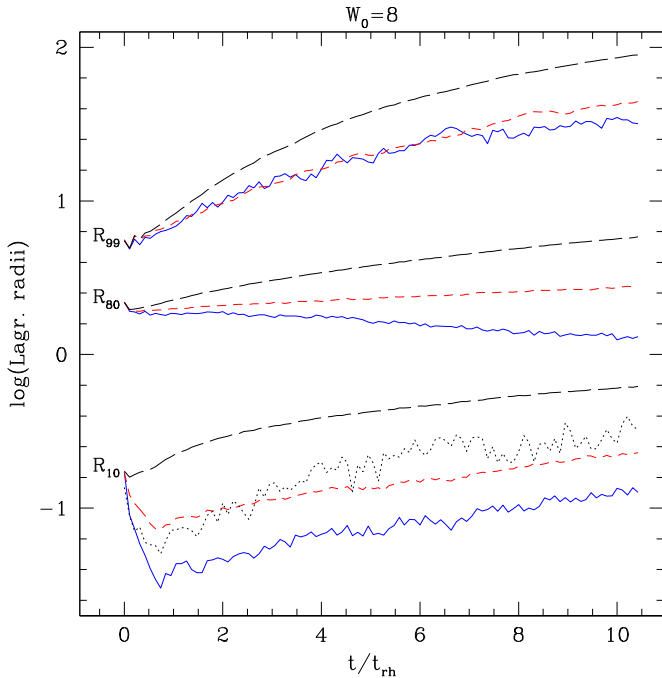
3.2. Results

Before going further into describing the BSS radial distribution resulting from the N-body approach, it is worth analyzing the overall evolution of the simulated stellar systems. In Figures 4–6, the evolution of three representative Lagrangian radii (R_p, with p being the percentage of the total mass they enclose in three dimensions) is reported for the three mass components and for each of the considered W_0 values, while Figure 7 refers to the $N = 10^5$, $W_0 = 8$ case. We chose R_{10}, which roughly measures the size of the core region, R_{99}, which corresponds to the very outer halo, and an intermediate Lagrangian radius delimiting a region of the cluster not

---

[8] While only *single* stars are generated in the initial conditions of the simulations, binary and multiple systems can form dynamically during the evolution.

[9] This number actually refers to the beginning of the simulations, for a certain fraction of stars escapes from the system during its evolution (because of evaporation and/or ejection).
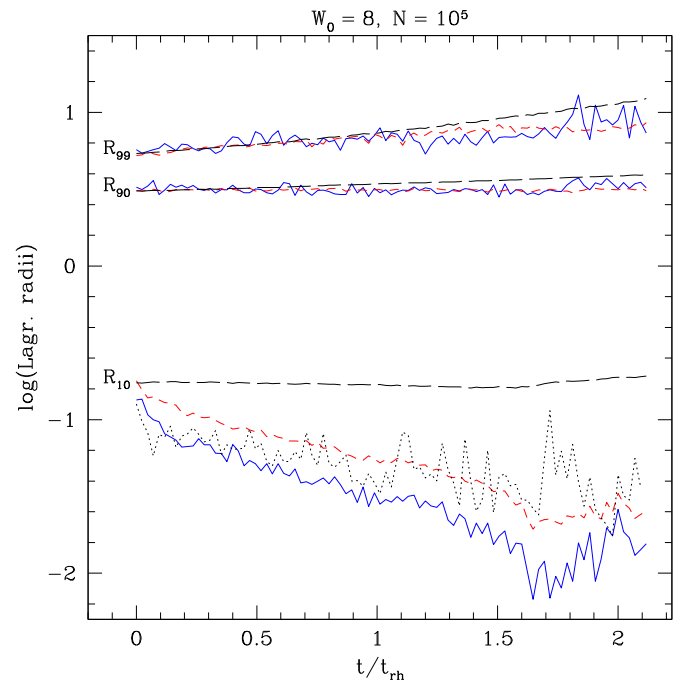
Figure 5. As in Figure 4 for the simulations started with $W_0 = 6$.

Figure 6. As in Figure 4 for the simulations started with $W_0 = 8$.

Figure 7. Same as in Figure 6 for the simulation with $N = 10^5$ stars, of which $N_{\rm BSS} = 300$, $N_{\rm ref} = 3000$.

especially in the central denser region. Incidentally, this mechanism also explains the apparent lack of core-contraction for the (lighter) field stars (their R_{10} is never contracting), which is due to the injection of kinetic energy from the contracting cores of the heavier components.

In the same figures, we also report (as dotted lines) the time evolution of the core radius of the reference population. To be as close as possible to the observational procedures adopted for real clusters, we searched for the best-fit King model to the central portion of the projected number density profile of the reference population and we defined $r_{\rm c}$ as the radius at which the surface density drops to half its central value. This corresponds well to the core radius adopted in observational works and it allows a meaningful comparison among BSS radial distributions determined in different GCs (see Ferraro et al. 2012). The behavior of $r_{\rm c}$ is close to that of R_{10}: it shows a well-defined contraction phase, followed by an expansion. The relatively sudden turnaround of $r_{\rm c}$ and R_{10} flags the onset of the so-called the CC process.

It can be seen that in our 10^4 particle N-body simulations, the CC phase starts at $t_{\rm CC}/t_{\rm rh} \simeq 3.7, 2.5, 0.7$ for $W_0 = 4, 6, 8$, respectively. As expected, the CC time is anti-correlated with the initial cluster concentration (i.e., with the collision rate in the core; see the "heavy tracers" case in Fregeau et al. 2002). However, we point out that the particular values of $t_{\rm CC}/t_{\rm rh}$ are not meant to be used for a close comparison with observational data since they are specific to the simplified initial conditions adopted here. In fact, the evolution of the simulated systems is unrealistically influenced by the heaviest components, which are largely overabundant ($N_{\rm BSS}/N_{\rm ref} \sim 0.25$ and $N_{\rm ref}/N_{\rm MS} \sim 0.14$) with respect to reality. Indeed, it is well known that, in general, the higher these ratios, the faster the collisional relaxation and the earlier the CC time, compared to the single-component case (see, e.g., the comprehensive discussion in Section 1.2 of Gürkan et al. 2004, and references therein; see also Table 2 of Fregeau et al. 2002). Thus, it is reasonable to expect that in a real GC,

participating to the late expansion phase of the system. Their behaviors essentially confirm those expected from the known collisional relaxation processes in multi-mass systems, of which extensive descriptions can be found in the literature (e.g., Heggie & Hut 2003; Gürkan et al. 2004; Khalisi et al. 2007, and references therein). Here, it is worth pointing out that the heavier components evolve toward a core-contraction (R_{10} decreases), while the halo (R_{99}) monotonically expands, with the evolutionary timescale being shorter for the heavier mass components (see Equation (1)). The halo expansion occurs mainly because the kinetic energy of (dynamically "cold") halo stars increases during *close* encounters with ("hot") core stars,

where the total stellar mass in BSSs and reference populations relative to the total cluster mass is much lower than in our N-body models, the evolution is comparably closer to that of a single-component system, characterized by a later core-contraction phase.

This is indeed confirmed by the $N = 10^5$ simulation results, where the number ratios among the different populations are more realistic. As shown in Figure 7, the CC time in this simulation is increased by a factor of 2.3 ($t_{CC}/t_{rh} \simeq 1.6$ for $W_0 = 8$) with respect to the 10^4 particle case. This comparison clearly shows that the 10^4 particle simulations presented here are too rough to provide accurate estimates of the characteristic timescales of the various dynamical processes. However, they can be used to investigate interesting trends and draw qualitative conclusions. The analysis of the trends shown in Figures 4–6 is indeed quite instructive.

In particular, the behavior of the Lagrangian radii as a function of time nicely highlights the properties of environmental conditions in which DF operates in real clusters. In fact, at odds with the static environment considered in the semi-analytical model, real clusters have time evolving environments where DF drifts heavy stars toward the center, first, in a contracting core (until the CC occurs), and then in an expanding core (after the CC). Thus, in the late evolutionary stages, DF can be somehow contrasted by the core expansion. However, it is worth noticing that R_{10} for the BSS population is significantly smaller than the typical size of the central peak in observational studies. Hence its time behavior (which is qualitatively similar to that of R_{10} and r_c for the reference population) is not expected to have a significant impact on the overall shape of the BSS distribution, apart from a possible increase of the width of the peak and a stabilization of its height in the post-CC regime.

3.3. Formation of the Bimodal Behavior

Within the "evolutionary" picture described above, we now examine the R_{BSS} profiles of the simulated N-body systems and compare them to that obtained from the semi-analytical model and the observations. The single super-snapshot shows a noisy behavior, hindering the automatic analysis of the BSS distribution, which risks losing important features (such as the depth of the minimum) and failing to achieve a reliable evaluation of the bimodality. For this reason, we used the adaptive binning procedure described in Section 2.3 to build the R_{BSS} profiles. The prescriptions adopted to determine the location of the minimum (r_{min}) and to evaluate the bimodality level (b) can also be found in that section. According to the observations, the distance from the cluster center was scaled to the instantaneous value of r_c, which was computed as described above.

In the lowest concentration case ($W_0 = 4$, not shown here) a central peak in the BSS radial distribution is soon developed and the external portion of $R_{BSS}(r)$ rapidly decreases without forming a significantly bimodal pattern. This can be understood by the fact that the timescale of the frictional decay depends predominantly on the density of the field stars (e.g., Alessandrini et al. 2014), and this density decreases more gradually with radius in low concentration clusters than in those highly concentrated. Hence, in the case of $W_0 = 4$, the DF timescale increases more slowly outward (i.e., its efficiency keeps relatively high up to a larger radius) than for $W_0 = 6, 8$. This can be seen in Figures 4–6, by comparing the slope of the inner Lagrangian radius behavior with that of the intermediate radius for the BSSs in the pre-CC phase. It is evident that in the
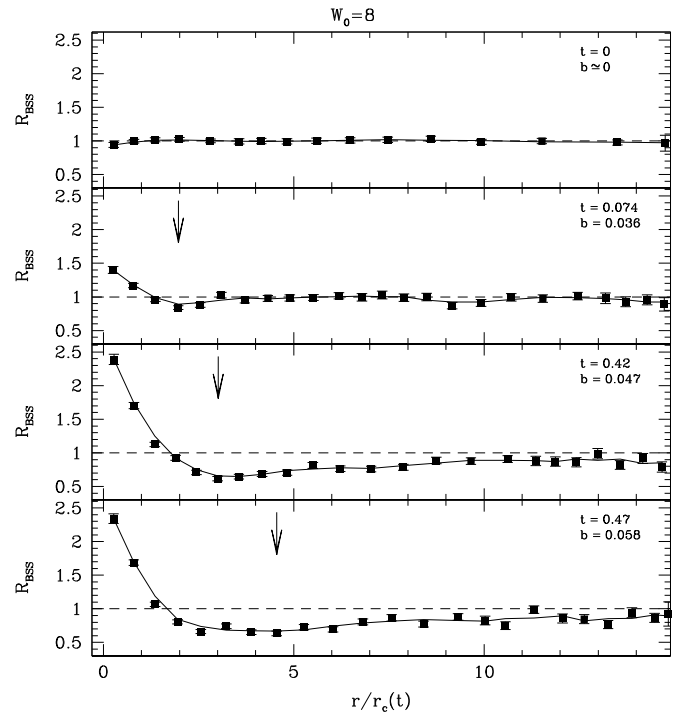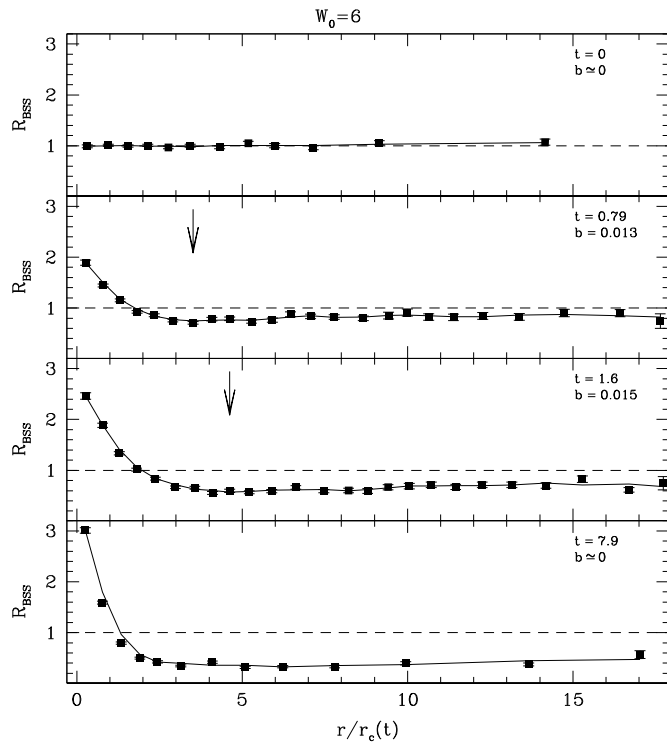

Figure 8. R_{BSS} profile (dots) for the N-body simulations starting with $W_0 = 8$, at different evolutionary times (see the labels). Dashed line: initial (unsegregated) value of R_{BSS}. The solid curve is the running average of R_{BSS} and the bimodality indicator (b) is also reported. The arrow marks the location of the absolute minimum, r_{min}.

$W_0 = 4$ case the trends of these two radii show more similar slopes than for $W_0 = 6, 8$. This means that in the $W_0 = 4$ model the BSSs decay at a rate that is almost independent of the radius (at least up to R_{90}), thus causing the double-normalized ratio to evolve very quickly toward the unimodal pattern. In fact, in order to ensure the persistence of a bimodal distribution, the BSSs orbiting in the outskirts have to decay much more slowly than those orbiting in the inner region.
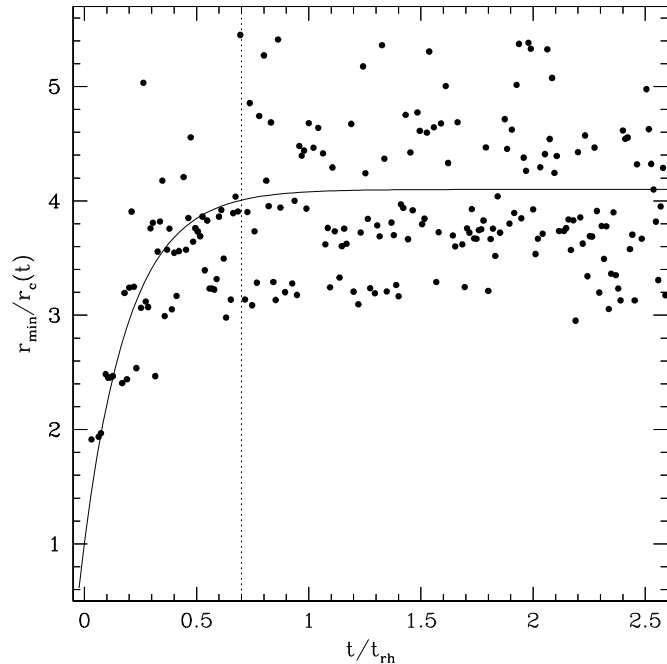
Representative examples of the radial distributions obtained in simulations with initial potentials $W_0 = 8$ and $W_0 = 6$ are shown in Figures 8 and 9, respectively, for the labeled evolutionary times (in units of the initial t_{rh}). By construction, $R_{BSS}(r)$ is nearly constant and close to unity at the initial time. As the evolution proceeds, a bimodal behavior develops, with an increasingly high central peak and a dip at intermediate radii (see also Figure 10). A number of interesting features can be inferred from these simulations:

1. all snapshots show the formation of a sharp central peak in the BSS radial distribution, regardless of the initial value of W_0 (including $W_0 = 4$);
2. at odds with the findings of the semi-analytical models the central peak is a quite stable feature;
3. the number of BSSs that drift to the center, because of the effect of DF, increases as a function of time;
4. in many cases, the BSS distribution is bimodal (Figure 10). This effect is somehow mitigated by a progressive decrease of N_{BSS} in the external regions, which makes the detection of bimodality difficult and needs to be further investigated;
5. the width of the dip seems to increase as a function of time, in good agreement with the observations;
6. in the latest snapshots, the simulated BSS distribution shows a monotonic behavior, with most of the BSSs segregated in the central part and the external radial bins
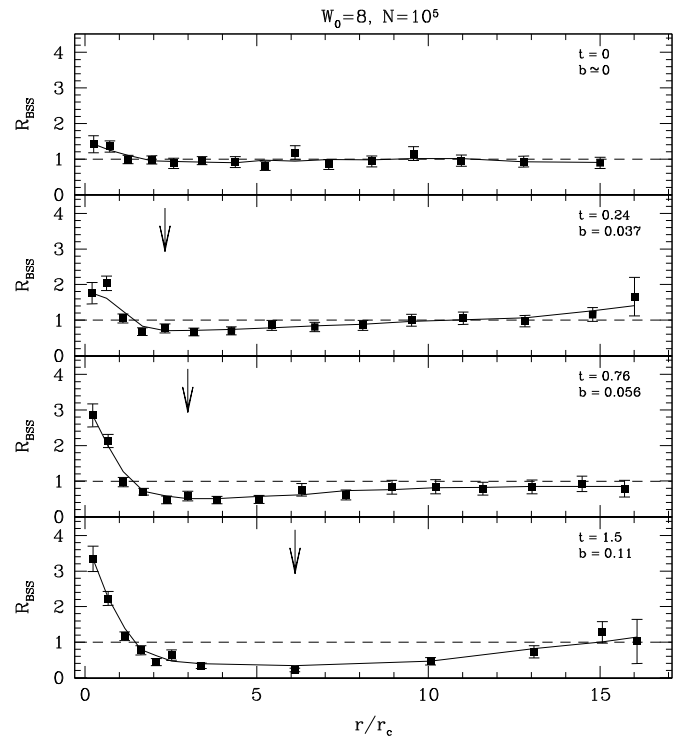
Figure 9. Same as in Figure 8 for the N-body simulations starting with $W_0 = 6$.

Figure 11. R_{BSS} profiles at different evolutionary times for the simulation run with $N = 10^5$ and $W_0 = 8$. Symbols and labels are the same as in Figure 8.

Figure 10. Time evolution of the position of the absolute minimum of the R_{BSS} profile (dots), in units of the instantaneous core radius, for the simulations started with $W_0 = 8$. A fitting exponential law ($\sim 1 - \exp(5t/t_{rh})$) is shown as a solid curve. Only R_{BSS} profiles for which $b > 0.01$ have been considered (see the text). The dotted line indicates t_{cc}, the time of the core-collapse.

Remarkably, the shape and width of the central peaks in Figures 8 and 9 are also very similar to those observed in real clusters belonging to Family II (i.e., those actually showing a bimodal BSS distribution; see Ferraro et al. 2012). In fact, as is apparent in their Figure 2, the large majority ($\sim 85\%$) of these systems have r_{min} smaller than $10 r_c$, consistently with the results of both our simulations with concentrated initial conditions and with the semi-analytical model results.

These results seem to be confirmed (at least qualitatively) by the R_{BSS} profiles obtained from the more realistic simulation run with $N = 10^5$ and starting with $W_0 = 8$ (see Figure 11), which will be deeply investigated and discussed in a forthcoming paper.

4. DISCUSSION AND CONCLUSIONS

In this paper, we have presented the results of a number of simulations aimed at exploring the connection between the evolution of the BSS spatial distribution and the cluster dynamical age. In this first study, we adopted simplified initial conditions and the simulations are not meant for a detailed and direct comparison with observational data but, rather, the goal was to explore the fundamental dynamical aspects driving the evolution of the BSS spatial distribution. Our results show a few features in nice qualitative agreement with observations and suggest that the dynamical mechanisms explored in this paper provide a promising route for the interpretation and understanding of the empirical dynamical clock found in our previous studies.

Our main result is that, because of the effect of DF, the BSS radial distribution develops a central peak and a minimum independently of the initial cluster concentration. In particular, the semi-analytical model (which, among all of the possible dynamical processes, takes into account DF only), shows the rapid formation of a bimodal distribution with a dip progressively moving toward the external regions of the cluster.

being essentially devoid of BSSs (see the bottom panel of Figure 9), in agreement with the BSS distributions observed in Family III clusters (Ferraro et al. 2012);

7. in the cases where the bimodality is clearly distinguishable, an outward drift of the dip for increasing evolutionary time is seen before the CC phase (see Figure 10).

However, this model fails to reproduce the formation of a long-lived central peak, which is instead observed in all dynamically evolved clusters (Ferraro et al. 2012). The results obtained from (preliminary) *N*-body simulations show the formation of a sharp and stable central peak and the development of a dip in the BSS radial distribution, regardless of the initial W_0. In spite of the noisy behavior of the snapshots, it can be stated that a bimodal distribution is set in many cases and the size of the dip tends to increase as a function of time until (in the latest evolutionary phases) the distribution becomes monotonic (in full agreement with the observations).

It is worth recalling the main differences between the two approaches we followed. (1) In the semi-analytical approach, the distribution of field stars is *static*, while, in the *N*-body simulations, the field component evolves self-consistently with time, following the core contraction and, especially, the halo expansion. (2) in the *N*-body system, various collisional phenomena originating from two-body and three-body interactions with *small* impact parameters are acting during the entire evolution, while the semi-analytical model takes into account only the DF effect (i.e.,the consequence of two-body interactions with *large* impact parameters). Despite the higher degree of realism of the *N*-body approach, from the dynamical point of view, the performed simulations are far from being representative of real clusters because of a number of particles that is too small (10^4) and an unrealistically high fraction of heavy species (especially BSSs) with respect to the lighter background component. The main effect of these limitations is to induce a global evolution of the system that is too fast (see Figures 6 and 7), producing unrealistically short dynamical timescales for the simulated clusters, especially in the lowest concentration ($W_0 = 4$) case. Thus, it is very possible that the low-mass stars (which are mainly responsible for the DF action on the test stars) in a real GC behave much more like the static background in the semi-analytical, DF-only approach, than in our (small) *N*-body simulations (see the long dashed curves in Figures 6 and 7).

More realistic simulations are therefore necessary to investigate this possibility and to properly follow the time evolution of the BSS radial distribution. In fact, while hints of a progressive outward movement of r_{min} are found in some of the simulations presented here, no reliable constraints can be obtained about the characteristic timescales of this process and the precise way the shape of the dip changes with time and the external cluster regions become devoid of BSSs. More realistic simulations are also needed to clarify exactly which are the internal "engines" of the dynamical clock. The preliminary results presented here clearly point out that DF is able to set the peak and the dip in the BSS distribution. However, we still have to determine which is the dominant phenomenon (and in what regime) that is able to drift r_{min} toward the external cluster regions (either DF only, or also the core expansion after the CC, or further dynamical processes). Certainly, the presence of primordial binaries and an external tidal field should also be taken into account because the former would presumably favor a smoother collisional evolution of the system (by mitigating CC) and the latter would limit the expansion of the low-mass stars halo. These more realistic *N*-body simulations are in progress and will be described in forthcoming papers.

APPENDIX

DYNAMICAL FRICTION IN A PLUMMER DISTRIBUTION FUNCTION

The semi-analytical treatment of DF of Section 2 is based on a numeric calculation of the deceleration suffered by a star on a given orbit in a Plummer potential. In the following, we provide all of the relevant details.

The distribution function leading to the Plummer model, with total mass M and characteristic radius r_0, is

$$f(r, v) = k \left[-\psi(r) - \frac{v^2}{2} \right]^{7/2}, \qquad (A1)$$

with k a normalization constant and

$$\psi(r) = -\frac{GM}{\sqrt{r^2 + r_0^2}} \qquad (A2)$$

the gravitational potential. The corresponding mass density generating this potential is

$$\rho(r) = \frac{\rho_0 r_0^5}{(r^2 + r_0^2)^{5/2}} = -\frac{\psi^5 \rho_0}{\sigma^{10}}, \qquad (A3)$$

with $\rho_0 \equiv 3M/4\pi r_0^3$ being the central density and $\sigma \equiv (GM/r_0)^{1/2}$ a characteristic velocity. Thus, the integral in Equation (3) yields

$$g(r, v) = -4\pi 2^{3/2} k \psi^5 \int_0^{v(-2\psi)^{-1/2}} w^2 (1 - w^2)^{7/2} \mathrm{d}w$$

$$= -4\pi 2^{3/2} k \psi^5 \int_u^\infty y^8 (1 + y^2)^{-6} \mathrm{d}y, \qquad (A4)$$

where the substitutions $w = v(-2\psi)^{-1/2}$, $y = (w^{-2} - 1)^{1/2}$ have been applied and $u \equiv (-2\psi v^{-2} - 1)^{1/2}$. The last integral gives

$$g(r, v) = g(\psi, u) = \alpha \psi^5 \left[\frac{1}{2} \tan^{-1}(u) \right.$$

$$\left. + \left(\frac{u^9}{2} - \frac{79}{21} u^7 - \frac{64}{15} u^5 - \frac{7}{3} u^3 - \frac{u}{2} \right)(1 + u^2)^{-5} - \frac{\pi}{4} \right],$$

$$(A5)$$

with $\alpha \equiv 7\pi \sqrt{2} k/16$.

In order to determine k and then α, from Equation (3) applied to the escape velocity ($u = 0$), we note that

$$\rho(r) = mg(\psi, 0) = -\frac{7\sqrt{2}}{64} \pi^2 m \psi^5 k. \qquad (A6)$$

Thus, comparison with Equation (A3) implies that $k = 32\sqrt{2}\rho_0(7\pi^2 m\sigma^{10})^{-1}$ and $\alpha = 4\rho_0(\pi m\sigma^{10})^{-1}$.

REFERENCES

Aarseth, S. J. 2003, Gravitational N-Body Simulations (Cambridge: Cambridge Univ. Press)

Alessandrini, E., Lanzoni, B., Miocchi, P., Ciotti, L., & Ferraro, F. R. 2014, ApJ, 795, 169

Bailyn, C. D. 1992, ApJ, 392, 519

Bailyn, C. D. 1995, ARA&A, 33, 133

Beccari, G., Dalessandro, E., Lanzoni, B., et al. 2013, ApJ, 776, 60

Beccari, G., Sollima, A., Ferraro, F. R., et al. 2011, ApJL, 737, L3

Bellazzini, M., Pasquali, A., Federici, L., Ferraro, F. R., & Pecci, F. F. 1995, ApJ, 439, 687

Binney, J. J., & Tremaine, S. 1987, Galactic Dynamics (Princeton, NJ: Princeton Univ. Press)

Chandrasekhar, S. 1943, ApJ, 97, 255

Chatterjee, S., Rasio, F. A., Sills, A., & Glebbeek, E. 2013, ApJ, 777, 106

Contreras Ramos, R., Ferraro, F. R., Dalessandro, E., Lanzoni, B., & Rood, R. T. 2012, ApJ, 748, 91

Dalessandro, E., Ferraro, F. R., Lanzoni, B., et al. 2013a, ApJ, 770, 45

Dalessandro, E., Ferraro, F. R., Massari, D., et al. 2013b, ApJ, 778, 135

Dalessandro, E., Lanzoni, B., Ferraro, F. R., et al. 2008, ApJ, 681, 311

Davies, M. B., Piotto, G., & de Angeli, F. 2004, MNRAS, 349, 129

De Marco, O., Shara, M. M., Zurek, D., et al. 2005, ApJ, 632, 894

Ferraro, F. R., Beccari, G., Dalessandro, E., et al. 2009, Natur, 462, 1028

Ferraro, F. R., D'Amico, N., Possenti, A., Mignani, R. P., & Paltrinieri, B. 2001, ApJ, 561, 337

Ferraro, F. R., Fusi Pecci, F., & Bellazzini, M. 1995, A&A, 294, 80

Ferraro, F. R., Fusi Pecci, F., & Buonanno, R. 1992, MNRAS, 256, 376

Ferraro, F. R., Fusi Pecci, F., Cacciari, C., et al. 1993, AJ, 106, 2324

Ferraro, F. R., Lanzoni, B., Dalessandro, E., et al. 2012, Natur, 492, 393

Ferraro, F. R., Paltrinieri, B., Rood, R. T., & Dorman, B. 1999, ApJ, 522, 983

Ferraro, F. R., Sabbi, E., Gratton, R., et al. 2006a, ApJL, 647, L53

Ferraro, F. R., Sills, A., Rood, R. T., Paltrinieri, B., & Buonanno, R. 2003, ApJ, 588, 464

Ferraro, F. R., Sollima, A., Rood, R. T., et al. 2006b, ApJ, 638, 433

Fiorentino, G., Lanzoni, B., Dalessandro, E., et al. 2014, ApJ, 783, 34

Fregeau, J. M., Joshi, K. J., Portegies Zwart, S. F., & Rasio, F. A. 2002, ApJ, 570, 171

Fusi Pecci, F., Ferraro, F. R., Corsi, C. E., Cacciari, C., & Buonanno, R. 1992, AJ, 104, 1831

Geller, A. M., de Grijs, R., Li, C., & Hurley, J. R. 2013, ApJ, 779, 30

Giersz, M., & Heggie, D. C. 1994, MNRAS, 268, 257

Gilliland, R. L., Bono, G., Edmonds, P. D., et al. 1998, ApJ, 507, 818

Gürkan, M. A., Freitag, M., & Rasio, F. A. 2004, ApJ, 604, 632

Heggie, D. C., & Hut, P. 2003, The Gravitational Million-Body Problem (Cambridge: Cambridge Univ. Press)

Heggie, D. C., & Mathieu, R. D. 1986, in The Use of Supercomputers in Stellar Dynamics, ed. P. Hut & S. McMillan (New York: Springer), 233

Hills, J. G., & Day, C. A. 1976, ApL, 17, 87

Hockney, R. W., & Eastwood, J. W. 1988, Computer Simulation Using Particles (New York: Adam Hilger)

Hut, P., McMillan, S., & Romani, R. W. 1992, ApJ, 389, 527

Hypki, A., & Giersz, M. 2013, MNRAS, 429, 1221

Khalisi, E., Amaro-Seoane, P., & Spurzem, R. 2007, MNRAS, 374, 703

King, I. R. 1966, AJ, 71, 64

Knigge, C., Leigh, N., & Sills, A. 2009, Natur, 457, 288

Lanzoni, B., Dalessandro, E., Perina, S., et al. 2007a, ApJ, 670, 1065

Lanzoni, B., Sanna, N., Ferraro, F. R., et al. 2007b, ApJ, 663, 1040

Li, C., de Grijs, R., Deng, L., & Liu, X. 2013, ApJL, 770, L7

Lovisi, L., Mucciarelli, A., Lanzoni, B., et al. 2013, ApJ, 772, 148

Mapelli, M., Ripamonti, E., Battaglia, G., et al. 2009, MNRAS, 396, 1771

Mapelli, M., Sigurdsson, S., Colpi, M., et al. 2004, ApJ, 605, L29

Mapelli, M., Sigurdsson, S., Ferraro, F. R., et al. 2006, MNRAS, 373, 361

McCrea, W. H. 1964, MNRAS, 128, 147

Meylan, G., & Heggie, D. C. 1997, A&AR, 8, 1

Monelli, M., Cassisi, S., Mapelli, M., et al. 2012, ApJ, 744, 157

Paresce, F., de Marchi, G., & Ferraro, F. R. 1992, Natur, 360, 46

Plummer, H. C. 1911, MNRAS, 71, 460

Pooley, D., & Hut, P. 2006, ApJL, 646, L143

Ransom, S. M., Hessels, J. W. T., Stairs, I. H., et al. 2005, Sci, 307, 892

Sandage, A. R. 1953, AJ, 58, 61

Sanna, N., Dalessandro, E., Ferraro, F. R., et al. 2014, ApJ, 780, 90

Shara, M. M., Saffer, R. A., & Livio, M. 1997, ApJL, 489, L59

Sills, A., Glebbeek, E., Chatterjee, S., & Rasio, F. A. 2013, ApJ, 777, 105

Sollima, A., Lanzoni, B., Beccari, G., Ferraro, F. R., & Fusi Pecci, F. 2008, A&A, 481, 701

Zinn, R., & Searle, L. 1976, ApJ, 209, 734